Slurry Pipeline for fluid transients in pressurized conduits

Tarik Chakkour

Slurry Pipeline for fluid transients in pressurized conduits

Tarik Chakkour

Univ. Paris 13, UMR 6205, LAGA, F-93430 Villetaneuse , France

October 15, 2018

Abstract. In this paper, a one-dimensional three-fluid model is developed in Python. The physical model features a mass and momentum balance for each fluid. It allows to predict the pressure drop and flow patterns. The hydraulic transport of slurry system in horizontal tubes has been investigated. To simulate it dynamically, continuity and momentum equations used in applied engineering problem, are solved together. These equations are conveniently solved using the method of characteristics (MOC). The mumerical results from the numerical code model head and pressure losses. We test numerically the fitting of the model with the real physical problem.

Keywords: Slurry shield; Pipeline transport; homogeneous single-phase; method of characteristics.

1 Introduction

Numerous slurry transportation pipeline systems have been built in the past 10 years. The Khouribga mines 187 km cross-country slurry pipeline in Morocco has often been referred to as one of the most challenging projects in terms of operating complexity and system configuration. This mineral pipeline secures the continuous transport of phosphate pulp from Khouribga mines to the Jorf Phosphate Hub integrated processing platform, where it will be transformed into derivative products, while cutting down on several intermediate steps for its transport. The Maroc Central project will be launched soon and is due to be completed in August 2025. The major beneficiary from this project is the economic development of the region. Thus company OCP wish to preserve the countries water resources and its ecosystem is jointly fulfilled with the Group's social commitment as well as its contribution to the economic development of the regions harboring its activities.

The authors of this paper investigate the hydraulic transport of particles in tubes. First, F. Benkhaldoun built in [2] the mathematical model of water flows and the transport-diffusion processes of pollutants. In the sequel, T. Chakkour uses in [4] the modeling approaches (0D/1D) for numerical simulations in tubes with abrupt contraction on OpenFoam (simulation software CFD 3D). Many works focus on multiphase flow models in which the phases are strongly coupled. The main difficulties in these models are due to the interfaces between the phases, and the discontinuities associated to them (Ishii & Mishima in [10], 1984). The originality of this work is to present in simplified form a homogeneous single-phase model. The most important advantage of this model is the considerably smaller number of variables to be solved compared to the multiphase model. Then, numerical approximations are less made to simulate the transport of slurry utilising a single-phase model.

In this paper, with the construction of secondary pipelines connecting the washing plants to the head station. This pipeline will also have major implications on the Group's carbon footprint. The strategy is to preserve water resources, save energy and reduce pollution. A one-dimensional three-fluid model is established based on single-phase flow theory by considering the rheological properties of the fluid. Conceivably, numerical simulation has been widely used to study the characteristics of pipeline transportation and desirable results have been achieved. Subsequently, the transport of slurry over the pipeline is investigated through numerical simulation based on numerical code.

The pipeline was primarily perceived as a means of transporting different materials. In [12], the author deals with multiple simulation techniques that are used to simulate the operation of the Antamina pipeline system. In the present work, the slurry pipeline is designed to transport phosphate rock from

Khouribga's minings to the Jorf Lasfar chemicals plants, this 187 km long slurry pipeline is scheduled to be complete in 2025. The pipeline will generate substantial savings in transport cost, as well as in water and energy. We carried out a mathematical modeling on a number of parameters influencing the process of conducting phosphate through the pipeline. In this way, we have been interested in modeling the linear or regular load losses, the hydraulic gradient, the pressure in any point of the pipeline The result is grouped into the numerical code written in Python that can provide us the behavior of the pressure drops, and the piezometric line along the pipeline.

The paper is organized as follows. We start with description of the Mathematical model which is presented in detail with the assumptions, see section 2. The method of characteristics (MOC) with time marching procedure is employed for finding the solutions. In section 3, we study the Darcy friction factor that is solved from the Swamee-Jain equation. Next, we deals in section 4 with the numerical discrete method for solving the original continuity and momentum equations. We propose in section 5 physical steady-state solutions for only one fluid. By comparing with explicit solutions, independent-time state occurs, proving the validation of model. We investigate in sections 6 and 7, the unsteady-state with artificial conditions and without for three-fluid models. We show the main results of these models.

2 Method of Characteristics for transient flow

In this section the differential equations of motion and continuity are developed for liquid flow through a conical tube as well as for a cylindrical tube. In order to present these equations in their simplest form, the terms of lesser importance are omitted from the equations. Denoting by A the cross sectional area that the fluid crosses the tube. The area A is, in general, a function of x, which is the coordinate distance along the axis of the tube from the arbitrary origin. The tube is inclined with horizontal at an angle θ, positive when the elevation increases in the positive x direction.

The continuity and momentum equations form a pair of quasi-linear hyperbolic partial differential equations in terms of two dependant variables, discharge Q and hydraulic-grade-line elevation H sometimes called the piezometric head, or in short, the head. The continuity equation in terms of discharge $Q = VA$ instead of the flow velocity V and piezometric head H leads to:

$$\frac{\partial H}{\partial t} + \frac{Q}{A}\frac{\partial H}{\partial x} - \frac{Q}{A}\sin(\theta) + \frac{a^2}{gA}\frac{\partial Q}{\partial x} = 0, \tag{1}$$

in which a is the acoustic wave speed or a wave celerity of the fluid. The wavespeed describes the speed of pressure waves travelling through a fluid medium. The wavespeed in a closed conduit is directly determined by the physical properties of conduit and fluid. We present here the wave speed a that is a useful parameter for few special elastic conduits with Poisson's ratio μ of the material, in which the walls is relatively thick in comparison with diameter. In this condition the constant a depend on the property of the pipe which is the wall thickness e. The wave speed propagation a for transient flow condition in the pipe:

$$a = \sqrt{\frac{\frac{K}{\rho}}{1 + \frac{CKD}{Ee}}}, \tag{2}$$

where K and ρ are the bulk modulus of elasticity and mass density of the fluid, E is the Young modulus (modulus of elasticity) of the pipe material, and C the parameter for the pipe geometry and restraints that depends on the Poisson's ratio μ of the wall material and how well the pipe is supported. Three support situations for a thin pipeline are examined:

1. $C = 1 - \frac{\mu}{2}$, if pipe is anchored at its upstream end only
2. $C = 1 - \mu^2$, if pipe is anchored throughout against axial movement
3. $C = 1$, if pipe is anchored with expansion joints throughout

For a perfectly rigid pipe, E is infinite, and the wave celerity a is simplified to:

$$a = \sqrt{\frac{K}{\rho}}. \tag{3}$$

Equation (2) is only true for single phase fluids. For slurry, there are two ideas to express the wave celerity a for a solid-liquid mixture. The first one is that Kao and Wood [15] considered the surge problem, and developed a mathematical model for the surge pressure in terms of hindered particle drag coefficients in the liquid. They used the following wave celerity a:

$$a = \sqrt{\frac{\frac{C_s}{\rho_s} + \frac{C_f}{\rho_f}}{\frac{C_s}{K_s} + \frac{C_f}{K_f} + \frac{D}{Ee}}}, \tag{4}$$

where s and f represent respectively solid and fluid phases, C_s and C_f are volumetric concentration of solid and fluid respectively. It is assumed that the total volume can be expressed as the sum of the liquid and the solid volumes. Then, the sum of the volumetric concentration of solid C_s and fluid C_f is equal to 1. From this, equality (4) yields:

$$a = \sqrt{\frac{\frac{C_s}{\rho_s} + \frac{1-C_s}{\rho_f}}{\frac{C_s}{K_s} + \frac{1-C_s}{K_f} + \frac{D}{Ee}}}. \tag{5}$$

Bechteler and Vogel [1] criticised the physical meaningfulness of the density term in equation (5). Instead, they proposed the speed of sound expression below, in line with the choice of Thorley and Hwang [13]:

$$a = \sqrt{\frac{\frac{1}{\rho_s C_s + (1-C_s)\rho_f}}{\frac{C_s}{K_s} + \frac{1-C_s}{K_f} + \frac{D}{Ee}}}. \tag{6}$$

Here the mixture density ρ in terms of the fluid and solid densities is given by th following relation:

$$\rho = \rho_s C_s + (1 - C_s)\rho_f. \tag{7}$$

For most engineering applications, the convective acceleration term $\frac{Q}{A}\frac{\partial H}{\partial x}$ and the slope term $\frac{Q}{A}\sin(\theta)$, are very small compared to other terms, thus they may be neglected in equation (1) (chaudhry 1987). Hence, a simplified continuity equation is derived:

$$\frac{\partial H}{\partial t} + \frac{a^2}{gA}\frac{\partial Q}{\partial x} = 0. \tag{8}$$

In equation (8) the distance x and time t are the independent variables while the piezometric head H and discharge Q are the dependent variables and are functions of x and t. Similary as in derivation of the continuity equation, the equation of motion, can be derived by applying Newton's second law of motion that takes the following form:

$$\frac{\partial H}{\partial x} + \frac{1}{gA}\frac{\partial Q}{\partial t} + \frac{Q}{gA^2}\frac{\partial Q}{\partial x} + \frac{fQ|Q|}{2gDA^2} = 0. \tag{9}$$

The equation of motion (9) is further simplified by dropping the convective acceleration term $\frac{Q}{gA^2}\frac{\partial Q}{\partial x}$ which is very small compared to other terms (chaudhry 1987). Hence, the equation (9) can be written in the following form:

$$\frac{\partial H}{\partial x}+\frac{1}{gA}\frac{\partial Q}{\partial t}+\frac{fQ|Q|}{2gDA^2}=0. \tag{10}$$

Water hammer equations described in [17] form a set of quasi-linear partial differential equations for there is no direct general solution. The standard method for solution of water hammer equations is the method of characteristics (MOC) which is developed by Wylie and Streeter [16].

The simplified equations of motion and continuity are identified as L_1 and L_2 (from equations (8) and (10)) and are combined linearly using an known multiplier λ. The terms L_1 and L_2 are just labels for the equations, and are used in the following linear combination to lead:

$$L=\lambda L_1+L_2=\lambda\left[\frac{g}{\lambda}\frac{\partial H}{\partial x}+\frac{\partial H}{\partial t}\right]+\frac{1}{A}\left[\frac{g}{\lambda}\frac{\partial Q}{\partial x}+\frac{\partial Q}{\partial t}\right]+\frac{fQ|Q|}{2DA^2}=0. \tag{11}$$

If the variable x is a function of time t, then the dependent variables H and Q are expressed in terms of the total derivatives with respect to time:

$$\frac{dH}{dt}=\frac{\partial H}{\partial x}\frac{dx}{dt}+\frac{\partial H}{\partial t},\quad \frac{dQ}{dt}=\frac{\partial Q}{\partial x}\frac{dx}{dt}+\frac{\partial Q}{\partial t}. \tag{12}$$

Now, it is necessary to select two particular values of λ which are $\pm\frac{g}{a}$ in order to simplify equation (11) which becomes the ordinary differential equation:

$$\lambda\frac{dH}{dt}+\frac{1}{A}\frac{dQ}{dt}+\frac{fQ|Q|}{2DA^2}=0. \tag{13}$$

The transformation by the MOC method of equations (8) and (10) gives four ordinary differential equations. These equations are then expressed in finite difference form, using the method of specified time intervals, and solutions are carried out with use of the digital computer. The MOC method is a powerful method which is applied in most of the remainder of this treatment. This method has many advantages. The first one is the stability criteria which is firmly established. The second one is that very complex systems may be handled. The last one is for the best accuracy of this method.

When the positive value λ is used, the straight line on the xt plane is called the positive characteristic line and is noted C^+, along which equation (13) is valid. This line C^+ is interpreted as a wave moving in the positive x direction, that is holding the line constant, as t decreases, x must increase at the rate at. A similar parallelism exists for the neagtive λ which permits to define the negative characteristic line C^-. The two compatibility equations are grouped and identified as C^+ and C^-:

$$C^+\begin{cases}\dfrac{g}{a}\dfrac{dH}{dt}+\dfrac{1}{A}\dfrac{dQ}{dt}+\dfrac{fQ|Q|}{2DA^2}=0, & (14)\\ \dfrac{dx}{dt}=+a. & (15)\end{cases}$$

$$C^-\begin{cases}-\dfrac{g}{a}\dfrac{dH}{dt}+\dfrac{1}{A}\dfrac{dQ}{dt}+\dfrac{fQ|Q|}{2DA^2}=0, & (16)\\ \dfrac{dx}{dt}=-a. & (17)\end{cases}$$

The aim here is to generalize the MOC method of equations (1) and (9) which are identified as L_1 and L_2 without neglecting any terms. The similar linear combination given previously in relation (11) is applied to get:

$$L=\lambda L_1+L_2=\lambda\left[\left(\frac{g}{\lambda}+\frac{Q}{A}\right)\frac{\partial H}{\partial x}-\frac{Q}{A}\sin(\theta)+\frac{\partial H}{\partial t}\right]+\frac{1}{A}\left[\left(\frac{g}{\lambda}+\frac{Q}{A}\right)\frac{\partial Q}{\partial x}+\frac{\partial Q}{\partial t}\right]+\frac{fQ|Q|}{2DA^2}=0. \tag{18}$$

Using the total derivatives of variables H and Q given by (12), equality (18) becomes:

$$\lambda\left(\frac{dH}{dt}-\frac{Q}{A}\sin(\theta)\right)+\frac{1}{A}\frac{dQ}{dt}+\frac{fQ|Q|}{2DA^2}=0. \tag{19}$$

The characteristic lines C^+ and C^- are given as follows:

$$C^+\begin{cases}\dfrac{g}{a}\left(\dfrac{dH}{dt}-\dfrac{Q}{A}\sin(\theta)\right)+\dfrac{1}{A}\dfrac{dQ}{dt}+\dfrac{fQ|Q|}{2DA^2}=0, & (20)\\ \dfrac{dx}{dt}=\dfrac{Q}{A}+a. & (21)\end{cases}$$

$$C^-\begin{cases}-\dfrac{g}{a}\left(\dfrac{dH}{dt}-\dfrac{Q}{A}\sin(\theta)\right)+\dfrac{1}{A}\dfrac{dQ}{dt}+\dfrac{fQ|Q|}{2DA^2}=0, & (22)\\ \dfrac{dx}{dt}=\dfrac{Q}{A}-a. & (23)\end{cases}$$

3 The friction factor

In the present work, an effort has been made to give the asymptotic behavior of the quantity that is the friction factor f multiplied by the disharge square Q^2. This quantity is involved in the last term of motion's equation (9), taking into account the Reynolds number. We assume in this study that the friction factor would be a monotonic function of Reynolds number, leading to the proper result. We look for the proper asymptotic limit friction-disharge term fQ^2, when the flow is very laminar. This allows to understand how the elevation varies in this case. First, we recall that the Reynolds number Re is a quantity which engineers use to estimate if a fluid flow is laminar or turbulent. Re can be defined as (see [9] for details)

$$\mathrm{Re}=\frac{\rho QD}{A\mu}. \tag{24}$$

In the case of Bingham plastic fluids, another important dimensionless number highlighting the importance of yield stress is the Hedström number He, which is defined as (see [9])

$$\mathrm{He}=\frac{\rho D^2\tau_0}{\mu^2}, \tag{25}$$

where τ_o is the yield point or yield strength of fluid. The Reynolds number tells if the flow is laminar or turbulent. If the Reynolds number is smaller than the critical Reynolds number $\mathrm{R}e_{cr}$ which is often assumed to be 2300, i.e $\mathrm{R}e_{cr}=2300$, the flow is laminar. After the laminar flow regime follows the transition region. There the flow switches between laminar and turbulent randomly. When the Reynolds number reaches a certain value, the flow turns from transitional to turbulent. The transition region ends approximately at the Reynolds number 4000. For laminar flow $\mathrm{R}e<\mathrm{R}e_{cr}$, the friction factor f is a function of the Reynolds number only and is given by a Hagen-Poiseuille equation:

$$f=\frac{64}{\mathrm{Re}}. \tag{26}$$

Whereas for turbulent flow $\mathrm{Re}>4000$, the friction factor f depends on the average height of roughness projections of pipe wall. The friction factor f_w for water can be approximated using the Swamee and Jain's (1976) equation

$$f_w = 1.325\left[\ln\left(\frac{\epsilon}{3.7D} + \frac{5.74}{\mathrm{Re}^{0.9}}\right)\right]^{-2}, \tag{27}$$

in which ϵ is the average pipe wall roughness height. The equation (27) is used to solve directly for the Darcy-Weisbach friction factor for a full-flowing pipe. It approximates the implicit Colebrook-White equation. From this and according to (24), the friction factor f_w can be expressed in terms of the disharge Q:

$$f_w = 1.325\left[\ln\left(\frac{\epsilon}{3.7D} + \frac{\alpha}{Q^{0.9}}\right)\right]^{-2}, \tag{28}$$

in which the quantity α is given by:

$$\alpha = 5.74\left(\frac{A\mu}{\rho L}\right)^{0.9}. \tag{29}$$

Little work [11, 14] concerning flow structure of non-Newtonian slurries in different flow regimes has been published. The objective of this research [11] is to describe the transport of slurry in a large-scale pipe. The author investigates in [14] the Bingham plastic rheological equation for non-Newtonian slurries. Under the assumption that the water is air-free, this confirms its Newtonian behaviour because shear rate is constant. Then, the Colebrook-White equation is widely used to compute f_w based on its rheological characteristics (detailed below). However, the slurry is categorized as a homogeneous flow, and is non-Newtonian.

If the disharge Q is very small, the friction coeffecient f_w given by equality (28) guarantees a null friction-disharge term $f_w Q^2$. On the other hand, Darby and Melson [6] obtained an empirical relation which was developed by Darby and Melson [7]. The empirical formulae gives the the expression f_T in the turbulent flow regime. This expression is used for evaluating the Fanning friction factor in the present study, and is given by following equality:

$$f_T = 10^a \mathrm{Re}^{-0.193}, \tag{30}$$

where f_T is the turbulent flow friction factor and

$$a = -1.47\left[1 + 0.146e^{-2.9\times10^{-5}\mathrm{He}}\right]. \tag{31}$$

An exact description of friction loss for Bingham plastics was fully developed laminar pipe flow by Buckingham [3]. Buckingham-Reiner equation in a dimensionless form reads:

$$f_L = \frac{64}{\mathrm{Re}}\left[1 + \left(\frac{\mathrm{He}}{6.2218\mathrm{Re}}\right)^{0.958}\right]. \tag{32}$$

Equality (32) expresses the Fanning friction for slurry in laminar regime in terms of the Hedstorm number He, and the Bingham Reynolds number Re. Darby and Melson [6], in view of Churchil [5] and Usagi obtained a single equation for all flow regimes. The modified friction factor f evolved by these authors is the combination of friction factors expressed in laminar and turbuent regimes:

$$f_s = [f_L^m + f_T^m]^{\frac{1}{m}}, \tag{33}$$

where,

$$m = 1.7 + \frac{4000A\mu}{\rho QD}. \tag{34}$$

The detailed rheological characteristics for water-slurry are presented to predict the friction factors f_w and f_s. The physical properties are utilized in Figures 6 and 8, that are measurables, whose values describe a state of a physical system. These values are computed with only pipe inner diameters, i.e. $D = 0.9m$. The pipeline was assumed rough showing that the characteristics of the friction factor were different for laminar and turbulent flow. Then, its roughness ϵ is 2.10^{-5}. Now, we will explain how the Reynolds number for water-slurry is computed using equation (24). Once its density is determined, the Reynolds number is given. Density can be changed generally by changing either the pressure or the temperature. The effect of pressure and temperature on the densities of water-slurry is small. The density of water-slurry increases at low temperatures. The density ρ_w and the dynamic viscosity μ_w of water are given $10^3 kg/m^3$ and $10^{-3} Pa.s$, respectively, at standard temperature ($0°C$) and pressure (1 atm).

Note that, the slurry is considered as a mixture between very fine particles of phosphate and water. Even this mixture, the slurry behaves like a homogeneous fluid characterized by density ρ_s and viscosity μ_s. The phosphate dominates the flow with high concentration. In practice, the ratio of volumetric concentration of phosphate is 60% and of water is 40%. Setting the density of phosphate with $\rho_p = 2.10^3 kg/m^3$, and using the density ρ_w of water, equality (7) gives the mixture density $\rho_s = 1600 kg/m^3$. Considering that the dynamic plastic viscosity of the slurry varies between 0.006 and 0.0102, and typically limited to simulation the maximum value in simulation, i.e. $\mu_s = 0.0102 Pa.s$.

Multiplying the friction factor f_s defined by equality (33) with the disharge square Q^2:

$$f_s Q^2 = f_L Q^2 \mathrm{e}^{\frac{\ln\left(1+\left(\frac{f_T}{f_L}\right)^m\right)}{m}}. \tag{35}$$

Substituting expression (24) of the Reynolds number Re into coupled equations (30) and (32), we get:

$$\frac{f_T}{f_L} = \frac{10^a}{64}\left(\frac{\rho D}{A\mu}\right)^{0.807} \frac{Q^{0.807}}{1 + \left(\frac{\mathrm{He}A\mu}{6.2218\rho D}\right)^{0.958} \frac{1}{Q^{0.958}}}. \tag{36}$$

The equality (36) shows that quantity $\frac{f_T}{f_L}$ converges to zero when Q goes to zero. If $\frac{f_T}{f_L}$ tends towards zero, then, using an order 1 limited development of the natural logarithm function ln, we obtain the following expansion of function:

$$\frac{\ln\left(1+\left(\frac{f_T}{f_L}\right)^m\right)}{m} = \frac{1}{m} + \frac{f_T}{f_L} + O\left(\left(\frac{f_T}{f_L}\right)^2\right). \tag{37}$$

Since the laminar flow friction factor f_L is defined by (31), $f_L Q^2$ is expressed as:

$$f_L Q^2 = \frac{64A\mu Q}{\rho D}\left[1 + \left(\frac{\mathrm{He}A\mu}{6.2218\rho D}\right)^{0.958} \frac{1}{Q^{0.958}}\right], \tag{38}$$

showing the following equivalence,

$$f_L Q^2 \simeq \frac{64\mathrm{He}^{0.958}\left(A\mu\right)^{1.958} Q^{0.042}}{\left(6.2218\right)^{0.958}\left(\rho D\right)^{1.958}}. \tag{39}$$

From this, and according to equalitie (35), the expanded expression $f_s Q^2$ is obtained:

$$f_s Q^2 \simeq \frac{64\mathrm{He}^{0.958}\left(A\mu\right)^{1.958} Q^{0.042}}{\left(6.2218\right)^{0.958}\left(\rho D\right)^{1.958}}. \tag{40}$$

4 Finite-difference equations

This section deals with the numerical discrete method for solving the original partial differential equations. To proceed with the numerical solution, we devide the pipe length into N sub-intervals of equal length Δx as illustrated in Figure 1. The x domain starts at the pipe entrance $x_1 = 0$ and ends at the valve $x_{N+1} = L$. The variables H and Q are then computed in the discretized domain shown in Figure 1. Since we want the physical information from nodes x_1, x_2, ..., x_{N+1} to travel along the characteristic lines, a time-step size Δt is computed using following formula:

$$\Delta t = C_r \frac{\Delta x}{a}, \tag{41}$$

where the Courant number C_r must be less than or equal to 1 [8]. Thus, the size of Δx and the wave celerity a determine the size of our time interval. Defining the characteristic line C^+ by a line AP. Next, assuming that the variables Q and H are known at point A. The aim here is to know these variables at point P. For that, by multiplying equation (14) by $\frac{adt}{g}$, and by integrating between the limits A and P, the equation (14) is placed in following form:

$$\int_{H_A}^{H_P} dH + \frac{a}{gA}\int_{Q_A}^{Q_P} dQ + \frac{1}{2gDA^2}\int_{x_A}^{x_P} fQ|Q| = 0. \tag{42}$$

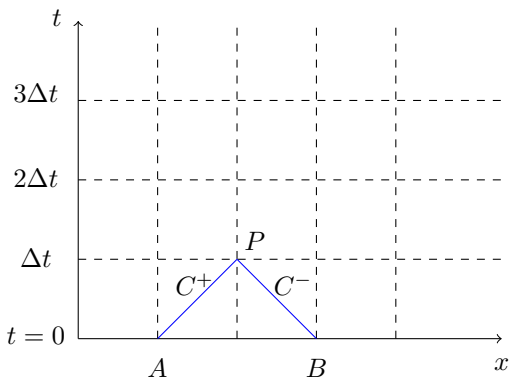

Figure 1: Numerical characteristics grid lines on the xt plane.

The similar integration along the characteristic line C^- defined by a line BP gives:

$$\int_{H_B}^{H_P} dH - \frac{a}{gA}\int_{Q_B}^{Q_P} dQ - \frac{1}{2gDA^2}\int_{x_B}^{x_P} fQ|Q| = 0. \tag{43}$$

The equations defined by relations (42) and (43) yield respectively:

$$H_P - H_A + \frac{a}{gA}(Q_P - Q_A) + \frac{f_A \Delta x}{2gDA^2} Q_A|Q_A| = 0. \tag{44}$$

$$H_P - H_B - \frac{a}{gA}(Q_P - Q_B) - \frac{f_B \Delta x}{2gDA^2} Q_B|Q_B| = 0. \tag{45}$$

By solving for H_P, these equations may be written:

$$C^+ : H_P = H_A - B(Q_P - Q_A) - R_A Q_A|Q_A|. \tag{46}$$

$$C^- : H_P = H_B + B(Q_P - Q_B) + R_B Q_B |Q_B|. \tag{47}$$

In equations (46) and (47), B is the Allievi constant, R_A and R_B are the resistance coefficients called the radius of gyration defined respectively at points A and B, which are given by:

$$B = \frac{a}{gA}, R_A = \frac{f_A \Delta x}{2gDA^2}, R_B = \frac{f_B \Delta x}{2gDA^2}. \tag{48}$$

We continue the same procedure for any interior grid point P_i in the x direction. Then, equations (46) and (47) take the simple following form:

$$C^+ : H_{P_i} = C_P - BQ_{P_i}, \tag{49}$$

$$C^- : H_{P_i} = C_M + BQ_{P_i}, \tag{50}$$

in which C_P and C_M are always known constants when the equations are applied:

$$C_P = H_{i-1} + BQ_{i-1} - R_{i-1}Q_{i-1}|Q_{i-1}|. \tag{51}$$

$$C_M = H_{i+1} - BQ_{i+1} + R_{i+1}Q_{i+1}|Q_{i+1}|. \tag{52}$$

By first summing equations (49) and (50), we get:

$$H_{P_i} = \frac{C_P + C_M}{2}. \tag{53}$$

Then, Q_{P_i} is found directly from either equation (49) or (50). The solution to a problem in liquid transients consists of finding the head H and the discharge Q for each grid point along $t = \Delta t$, then proceeding to $t = 2\Delta t$, until the final time.

5 Stationary solutions

The aim here is to determine the steady fluid flow. We give an explicit analytic representation of the stationary solutions of equations (8) and (10), and compare with the approximated solutions which are illustrated by the numerical simulations. The stationary solution still can be computed explicitly. Finally, we study the goodness of the approximations using the perturbation techniques.

5.1 Initial and boundary conditions

Boundary conditions are essentially a relationship between head H and discharge Q at a boundary node, which can then be solved with the characteristic equations to provide a full solution for the boundary. In the models the head-discharge relationship at the boundary can often be solved simultaneously with the appropriate characteristic equations to produce a direct solution. For the upsteram boundary, equation (50) is valid along C^-, and for downsteram boundary (49) is valid along C^+. Each boundary condition is solved independently of the other boundary, and independently of the interior point.

We use Dirichlet boundary condition to get the stationary solutions. We impose at the upstream and downstream ends the same value of disharge Q_0. We recall that x_1, x_2, ..., x_{N+1} are the nodes of the physical domain. Denoting the upstream boundary head $H(t_1, x_1)$ by $H(x_1)$, and the downstream boundary head $H(t_1, x_{N+1})$ by $H(x_{N+1})$. The quantity $H(x_{N+1})$ is expressed in terms of $H(x_1)$:

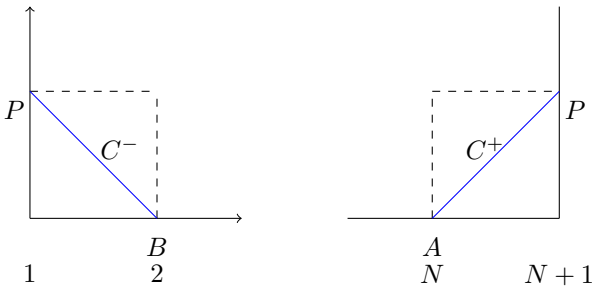

Figure 2: Characteristics at boundaries.

$$H(x_{N+1}) = H(x_1) - \frac{fLQ|Q|}{2gDA^2}. \tag{54}$$

Initializing the head H with constant $H(x_1)$, meaning that:

$$\forall i \in [\![1; N+1]\!], H_0(x_i) = H(x_1). \tag{55}$$

5.2 Exact solutions

Consider a fluid entering a circular pipe presented in Figure 4. A stationary state of the model is constituted by the conservative variables H and Q that remain in the same state. According to equation (8), if the head H is independent of time, then the disharge Q is constant in space. Otherwise, the disharge Q does not vary over time, the disharge Q is constant in space and time. In the steady-state, the disharge Q is equal to constant Q_0:

$$Q(t, x) = Q_0. \tag{56}$$

From this, equation (10) yields:

$$\frac{\partial H}{\partial x} = -\frac{fQ|Q|}{2gDA^2}, \tag{57}$$

which is coupled with equality (56) to get:

$$\frac{\partial H}{\partial x} = -\frac{fQ_0|Q_0|}{2gDA^2}. \tag{58}$$

We notice that the friction f depends on the disharge Q which is a constant. By integrating equation (57) between inferior bound x_1 and superior bound x, we get:

$$H(t, x) = H(x_1) - \frac{fQ_0|Q_0|}{2gDA^2}(x - x_1). \tag{59}$$

Equation (59) implies that the head H is an affine function of a decreasing slope. This equation can be given in the discrete form:

$$\forall i \in [\![2; N]\!], H(x_i) = H(x_1) - \frac{fQ_0|Q_0|}{2gDA^2}(x_i - x_1). \tag{60}$$

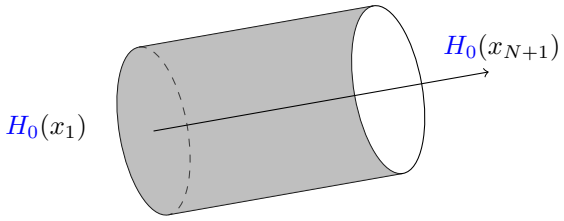

Figure 3: The flow of a fluid in a circular pipe.

We present the numerical results in Figure 5 that are shared into five pictures. The initial head H_0 is presented in picture 5a. The head generated by the numerical code using the method of characteristics is the same that is the exact one given by equality (59). It is concluded that these results are consistent with the model. Initializing discharge in 5c with the value Q_0. At the final stage of time, the numerical discharge Q is shown in picture 5d. The slant of view of this simulation is interpreted as follows. The discharge Q remains in the same state as time elapses, in every observable instant. This means that it is unchanging in time. Indeed, this discharge Q is equal to the constant Q_0 (see equality (56)). Now, setting a scale with precision near from 10^{-15}, the oscillatory movement appears, meaning of something physically happens. This discharge Q is presented in picture 5e. Consequently, the steady-state is approached asymptotically, proving that state variables are unchanging in continuous time.

6 Instationary solutions

This section essentially deals with the so-called three-fluid model. In this model, we focus on the study the instationary flow. The pipeline is divided into three sections. Consider a water streaming the first section which is defined between two points x_1 and x_{N_1+1}. Next, the slurry flows in the second one $[x_{N_1+1}, x_{N_2+1}]$. The water dominates the third section $[x_{N_2+1}, x_{N+1}]$ allowing the slurry to exit from the pipeline. We assume that there is no direct contact between water and slurry.

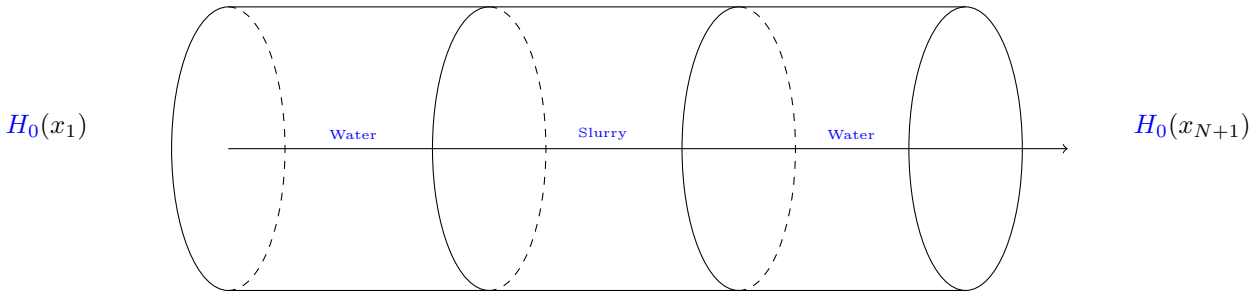

Figure 4: Schematics of water-slurry-water flow in a circular pipe.

The initial disharge Q_0 is defined by constant Q_0:

$$Q_0(x) = Q_0, \tag{61}$$

and the initial head H_0 is obtained by following equality:

$$H_0(x) = \begin{cases} H(x_1) - \frac{f_w Q_0|Q_0|}{2gDA^2}(x - x_1), & x \in [x_1, x_{N_1+1}], \\ H(x_1) - \frac{f_s Q_0|Q_0|}{2gDA^2}(x - x_1), & x \in [x_{N_1+1}, x_{N_2+1}], \\ H(x_1) - \frac{f_w Q_0|Q_0|}{2gDA^2}(x - x_1), & x \in [x_{N_2+1}, x_{N+1}], \end{cases} \tag{62}$$

in which f_w and f_s are the friction factors for water and slurry, which are computed according to equalities (28) and (34), respectively. The speeds of sound in water and slurry are given by quantities a_w and a_s, which are computed using equalities (2) and (4), respectively.

The nature of boundary conditions used here is explained as follows. We apply the Dirichlet boundary conditions for the variable H. The relation between the head H at the upstream boundary $H(x_1)$, and at the downstream boundary $H(x_{N+1})$ is given by the following equality:

$$H(x_{N+1}) = H(x_1) - \frac{f_w L Q_0|Q_0|}{2gDA^2}. \tag{63}$$

For the disharge Q, we impose the Neumann condition at the upstream boundary, on the contrary, the Dirichlet condition is adjusted at the downstream boundary.

Six targeted flashed images are illustrated in Figure 6 to simulate the unsteady-state of three-fluid flow. This head H_0 defined by equality (62) is shown in picture 6a. This initial head H_0 is a discontinuous function due to water's density being less than liquid slurry's. This comparison is justified by using equality (28). It is concluded that the friction coefficient f_w is less than the slurry one f_s, showing that the hydraulic-grade-line elevation for slurry is under water.

The interpretation of the simulation defined in pictures 6b and 6c are given as follows. The flow is shared into two parts. The first one L_1 is constitued with left water and slurry. The mixture of these two liquids forms one having an elevation which is close to slurry one. This liquid goes to the left side and reflectes. The second one L_2 is constitued with slurry and right water. The fluide's particules generated by this mixture move over the pipeline. At time 84, the interaction between liquids L_1 and L_2 give fluide's particules that are ready to leave the right side. The picture 6c shows that these particules exit the pipeline at instant $T_{\max}$. Only one mixture of liquids L_1 and L_2 dominates the flow generating one fluid at the final time.

Now, we give how the disharge varies in pictures 6d, 6e and 6f. Setting the initial disharge Q_0 to value $\frac{10}{9}$, i.e. $Q_0 = \frac{10}{9}$. This disharge Q_0 defined by equality (61) is shown in picture 6d, meaning that is constant at initial time in terms of position's pipeline. In the begining of this simulation, the disharge is ever constant in the second region. It follows that at instant 84, the moving slurry's disharge is less than the water one (see picture 6e). The model converges to a piecewise function presented in picture 6f. It is allowing to generate the same discharge in the first and last regions, and greater one in the middle region.

Consequently, these researchs given by prictures 5 and 6 focussed on predicting pressure drop and discharge in cement slurries flow in circular pipe. Results showed that regime unsteady-state determine only one state in the final stage. This slurry was produced and evoluated over time in a mixing phosphate and water. The final state shows that the head is homogeneous. The combinations of these particles are correlated, that how this model fluid behavior is evaluated. Since single-phase fluid is pipelined at large distances, nonreacting particles are forming a sedimentation bed on the bottom of the pipeline. At instant $T_{\max}$, the sedimentation bed exit from the pipe. This confirming that the inlet and oulet discharge is the same, even it is a discontinuous function in space.

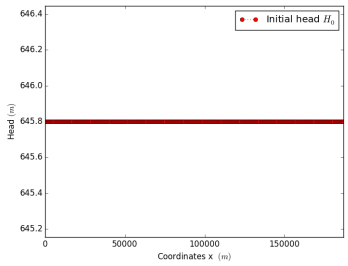

(a) Initial head $H_0(x)$.

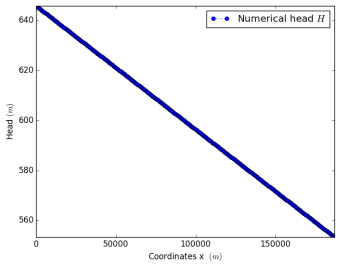

(b) Head $H(t,x)$ at $T_{\max}$.

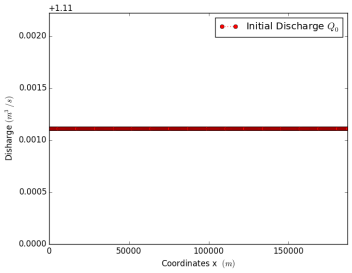

(c) Initial disharge $Q_0(x)$.

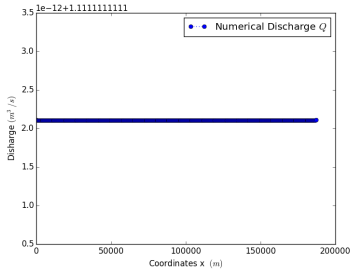

(d) Numerical disharge $Q(t,x)$ at $T_{\max}$.

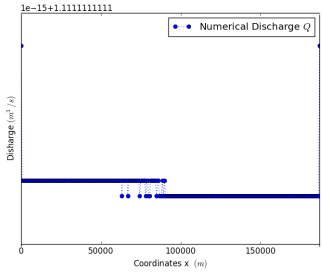

(e) Numerical disharge $Q(t,x)$ at $T_{\max}$.

Figure 5: Evolution of head-disharge over space in steady-state.

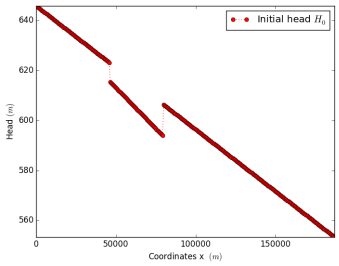

(a) Initial head $H_0(x)$.

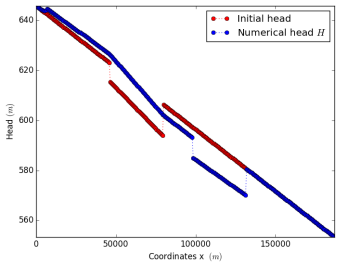

(b) Initial and numerical heads $H(t,x)$ at instant 84.

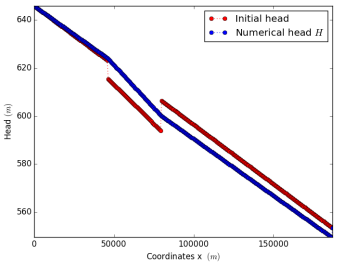

(c) Initial and numerical heads $H(t,x)$ at $T_{\max}$.

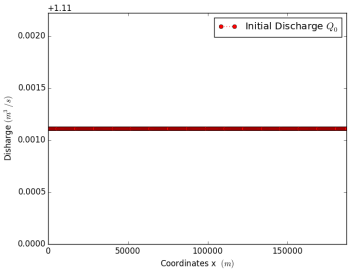

(d) Initial disharge $Q_0(x)$.

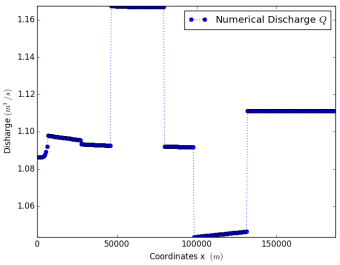

(e) Numerical disharge $Q(t,x)$ at instant 84.

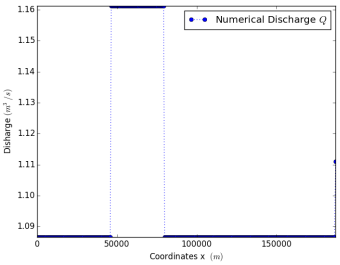

(f) Numerical disharge $Q(t,x)$ at $T_{\max}$.

Figure 6: Evolution of head-disharge over space in unsteady-state.

7 Coupling models

Unsteady flow in pipeline is the source for investigations which are many unwanted phenomenas. It is interesting in a pratical point of view. Unsteady flow model has been developed to describe transitional processes like single-phase flow in the pipeline. The pipeline is divided into three sections with keeping the same modeling in section 6 (see Figure 7). The difference that this model uses three artificial conditions at each parts of section. To simulate this model, equations (8) and (10) must be solved together in each section of the pipeline independently on other. These equations are solved using the method of characteristics.

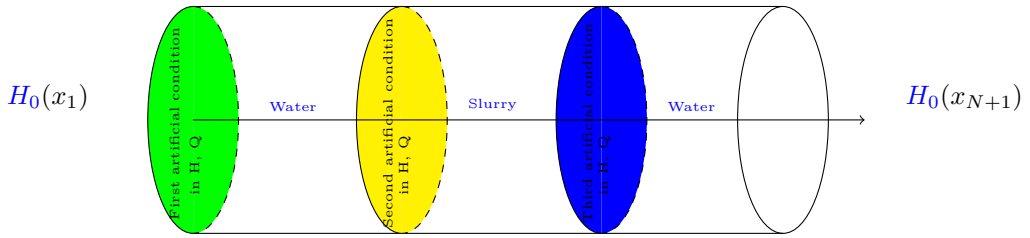

Figure 7: Schematics of water-slurry-water flow in a circular pipe with artificial conditions.

The initial disharge Q_0^i is defined by two constants Q_0 and Q_1:

$$Q_0^i(x) = \begin{cases} Q_0, & x \in [x_1, x_{N_1+1}], \\ Q_1, & x \in [x_{N_1+1}, x_{N_2+1}], \\ Q_0, & x \in [x_{N_2+1}, x_{N+1}], \end{cases} \tag{64}$$

and the initial head H_0^i is given by:

$$H_0^i(x) = \begin{cases} H(x_1), & x \in [x_1, x_{N_1+1}], \\ H(x_1) - \frac{f_s Q_1 |Q_1|}{2gDA^2}(x_{N_1+1} - x_1), & x \in [x_{N_1+1}, x_{N_2+1}], \\ H(x_1) - \frac{f_w Q_0 |Q_0|}{2gDA^2}(x_{N_2+1} - x_1), & x \in [x_{N_2+1}, x_{N+1}]. \end{cases} \tag{65}$$

We will apply the Dirichlet boundary conditions for the head H at the upstream boundary of each section. These upstream boundaries are given by quantities $H(x_1)$, $H(x_{N_1+1})$, and $H(x_{N_2+1})$ which are defined respectively by:

$$H(x_1) = H_0^i(x_1). \tag{66}$$

$$H(x_{N_1+1}) = H(x_1) - \frac{f_s Q_1 |Q_1|}{2gDA^2}(x_{N_1+1} - x_1). \tag{67}$$

$$H(x_{N_2+1}) = H(x_1) - \frac{f_w Q_1 |Q_1|}{2gDA^2}(x_{N_2+1} - x_1). \tag{68}$$

The head at the downstream boundary is defined by the Neumann condition at each parts of section. In what to follow, for the disharge Q, we impose the Neumann condition at the upstream boundary. On the contrary, the Dirichlet condition is adjusted at the downstream boundary.

The variation of head-disharge is shown in Figure 8 that is shared into four pictures. The initial head H_0 defined by equality (65) is shown in picture 8a. This head is a piecewise constant function, which is equal to $H(x_1)$ over the first region, to $H(x_1) - \frac{f_s Q_1 |Q_1|}{2gDA^2}(x_{N_1+1} - x_1)$ between positions x_{N_1+1} and x_{N_2+1} and to $H(x_1) - \frac{f_w Q_0 |Q_0|}{2gDA^2}(x_{N_2+1} - x_1)$ over the last region. The disharge is initialized according to equality (64), that is shown in the picture 8c, and its evolution until instant $T_{\max}$ is presented in the picture 8d. The head converges to a piecewise affine function at the final instant $T_{\max}$. The elevation of the three-fluid model is not the same, showing that the fluid is not homogeneous because of using three different artificial conditions. Noticing that we have showed in the steady-state that each constant head converges to an affine function of a decreasing slope. In the same case the disharge remains the same. The same reasoning is available for head and disharge constituting each piece, justifying this result. It is concluded that the unsteady flow converges to the stady-state, acheiving the validation of this model.

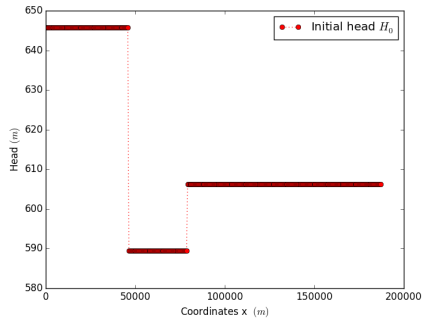

(a) Initial head $H_0(x)$.

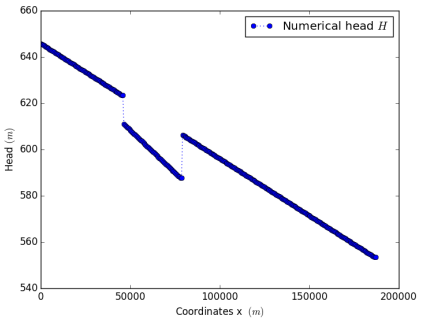

(b) Numerical head $H(t, x)$ at $T_{\max}$.

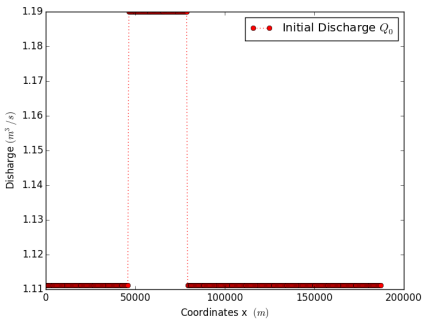

(c) Initial disharge $Q_0(x)$.

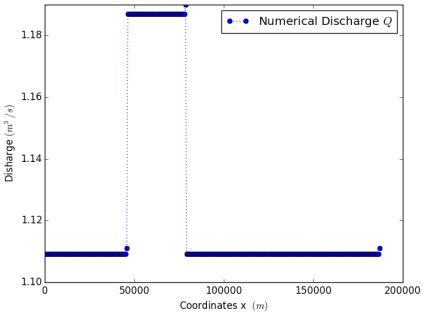

(d) Numerical disharge $Q(t, x)$ at $T_{\max}$.

Figure 8: Coupling models and evolution of head-disharge over space in unsteady-state.

References

[1] W Bechteler and G Vogel. Pressure wave velocity in slurry pipelines. In *Proc. of Hydrotransport*, volume 8, 1982.

[2] Fayssal Benkhaldoun, Imad Elmahi, Mohammed Seaı, et al. Well-balanced finite volume schemes for pollutant transport by shallow water equations on unstructured meshes. *Journal of computational physics*, 226(1):180–203, 2007.

[3] E Buckingham. On plastic flow through capillary tubes. In *Proc. Am. Soc. Testing Materials*, pages 1154–1156, 1921.

[4] Tarik Chakkour. Simulations numériques des tubes avec contraction brusque sur openfoam. *Thermodynamique des interfaces et mécanique des fluides*, 17, 2017.

[5] Stuart W Churchill. Friction-factor equation spans all fluid-flow regimes. *Chemical engineering*, 84(24):91–92, 1977.

[6] R Darby and J Melson. How to predict the friction factor for flow of bingham plastics. *Chemical Engineering*, 88(26):59–61, 1981.

[7] R Darby, R Mun, and DV Boger. Predict friction loss in slurry pipes. *Chemical Engineering*, 99(9):116–119, 1992.

[8] Robert J Fennema and M Hanif Chaudhry. Explicit numerical schemes for unsteady free-surface flows with shocks. *Water Resources Research*, 22(13):1923–1930, 1986.

[9] Marino Grozdek, Rahmatollah Khodabandeh, and Per Lundqvist. Experimental investigation of ice slurry flow pressure drop in horizontal tubes. *Experimental Thermal and Fluid Science*, 33(2):357–370, 2009.

[10] M Ishii and K Mishima. Two-fluid model and hydrodynamic constitutive relations. *Nuclear Engineering and design*, 82(2-3):107–126, 1984.

[11] Joel T Park, Richard J Mannheimer, Terrence A Grimley, and Thomas B Morrow. Pipe flow measurements of a transparent non-newtonian slurry. *Journal of fluids engineering*, 111(3):331–336, 1989.

[12] George Shou. Slurry pipeline system: Simulation and validation.

[13] ARD Thorley and LY Hwang. Effects of rapid change in flowrate of solid-liquid mixtures. In *Proceedings of Hydrotransport 6th Conference, UK*, pages 229–242, 1979.

[14] Richard W. Hanks and Bharat H. Dadia. Theoretical analysis of the turbulent flow of non-newtonian slurries in pipes. *AIChE Journal*, 1971.

[15] Don J Wood and TY Kao. Unsteady flow of solid-liquid suspensions. *Journal of the Engineering Mechanics Division*, 92(6):117–134, 1966.

[16] E Benjamin Wylie and Victor Lyle Streeter. Fluid transients. *New York, McGraw-Hill International Book Co., 1978. 401 p.*, 1978.

[17] E Benjamin Wylie, Victor Lyle Streeter, and Lisheng Suo. *Fluid transients in systems*, volume 1. Prentice Hall Englewood Cliffs, NJ, 1993.